Title

Seasonal variation of carbon monoxide in northern Japan: Fourier transform IR measurements and source-labeled model calculations

Journal

Journal of Geophysical Research-Atmospheres, 111(D15)

ISSN

0148-0227

Authors

Koike, M
Jones, N B
Palmer, P I
et al.

Publication Date

2006-08-01

DOI

10.1029/2005JD006643

March 6, 2006

Seasonal Variation of Carbon Monoxide in Northern Japan: FTIR Measurements and Source-labeled Model Calculations

M. Koike,[1] N. B. Jones,[2] P. I. Palmer,[3,4] H. Matsui,[1] Y. Zhao,[5] Y. Kondo,[6] Y. Matsumi,[7]

and H. Tanimoto[8]

[1] Department of Earth and Planetary Science, Graduate School of Science, The University of Tokyo, Tokyo, Japan (koike@eps.s.u-tokyo.ac.jp)
[2] Department of Chemistry, University of Wollongong, Wollongong, Australia
[3] Division of Engineering and Applied Sciences, Harvard University, Cambridge, MA, USA
[4]Now at the School of Earth and Environment, University of Leeds, Leeds, UK
[5] Mechanical and Aeronautical Engineering, University of California, Davis, CA, USA
[6] Research Center for Advanced Science and Technology, The University of Tokyo, Tokyo, Japan
[7] Solar-Terrestrial Environment Laboratory, Nagoya University, Aichi, Japan
[8] National Institute for Environmental Studies, Tsukuba, Ibaraki, Japan

Short title: KOIKE ET AL.: SEASONAL VARIATION OF CO IN JAPAN

Submitted to Journal of Geophysical Research, Atmospheres
Revised following the reviewers' comments.

Abstract. Tropospheric carbon monoxide (CO) was measured throughout 2001 using ground-based Fourier transform IR (FTIR) spectrometers at Moshiri (44.4°N) and Rikubetsu (43.5°N) observatories in northern Japan, which are separated by 150 km. Seasonal and day-to-day variations of CO are studied using these data, and contributions from various CO sources are evaluated using three-dimensional global chemistry transport model (GEOS-CHEM) calculations. Seasonal maximum and minimum FTIR-derived tropospheric CO amounts occurred in April and September, respectively. The ratio of partial column amounts between the 0-4- and 0-12-km altitude ranges is found to be slightly greater in early spring. The GEOS-CHEM model calculations generally reproduce these observed features. Source-labeled CO model calculations suggest that the observed seasonal variation is caused by seasonal contributions from various sources, in addition to a seasonal change in chemical CO loss by OH. Changes in meteorological fields largely control the relative importance of various source contributions. The contributions from fossil fuel (FF) combustion in Asia and photochemical CO production have the greatest yearly averaged contribution at 1 km among the CO sources (31% each). The Asian FF contribution increases from winter to summer, because weak southwesterly wind in summer brings more Asian pollutants to the observation sites. The seasonal variation from photochemical CO production is small (±17% at 1 km), likely due to concurrent increases (decreases) of photochemical production and loss rates in summer (winter), with the largest contribution between August and December. The contribution from inter-continental transport of European FF combustion CO is found to be comparable to that of Asian FF sources in winter. Northwesterly wind around the Siberian high in this season brings pollutants from Europe directly to Japan, in addition to southward transport of accumulated pollution from higher latitudes. The influences are generally greater at lower altitudes, resulting in a vertical gradient in the CO profile during winter. The model underestimates total CO by 12-14% between March and June. Satellite-derived

fire-count data and the relationship between FTIR-derived HCN and CO amounts are generally consistent with biomass burning influences, which could have been underestimated by the model calculations.

1. Introduction

Quantifying the continental outflow and inter-continental transport of pollutants is one of the major challenges of atmospheric chemistry. Quantitative evaluations require accurate information regarding emissions, transport processes, and photochemical transformations. Carbon monoxide (CO) has been used to test our current knowledge because it is a good tracer of combustion processes. The lifetime of CO is sufficiently long (10 days over continents in summer to over a year at high latitudes in winter [Holloway et al., 2000]) to study how transport redistributes pollutants on regional-to-hemispheric scales, and it is also sufficiently short that we can identify these impacts with a reasonably high signal-to-noise ratio. About half of the CO in the troposphere is estimated to have been emitted directly into the atmosphere, while the other half is produced by oxidation of methane (CH_4) and various anthropogenic and biogenic volatile organic compounds (VOCs) [e.g., *IPCC*, 2001]. Of the direct CO emissions, fossil and bio- fuel burning and biomass burning are estimated to be two dominant sources. Increases in anthropogenic emissions of CO can induce an interannual trend in the CO abundance, while biomass burning is considered to be a driver of year-to-year variation of CO over hemispheric scales [*Novelli et al*., 2003; *van der Werf et al*., 2004; *Yurganov et al*., 2005].

Because of the rapid economic growth and industrialization in the People's Republic of China and other Asian countries, understanding the influences from anthropogenic sources in these regions is of great importance. Impacts and transport pathways of Asian anthropogenic emissions and biomass burning have been studied using CO [e.g., *Bey et al*., 2001; *Liu et al*., 2003; *Liang et al*., 2004; *Bertschi and Jaffe*, 2005; *Oshima et al*., 2004]. Inverse modeling techniques have also been applied to estimate CO emission amounts in East Asia and other source regions using three-dimensional chemical transport models (CTMs) and ground-based, aircraft, and satellite measurements [*Palmer et al*., 2003; *Heald et al*., 2004; and references therein].

These studies have shown that recent emission inventories by *Streets et al*. [2003] likely underestimate anthropogenic CO emissions from China by half.

Quantitative understanding of anthropogenic influences on CO is especially important because of its critical role in controlling the oxidizing capacity of the atmosphere [*Logan et al*., 1981]. The oxidation process of CO to carbon dioxide (CO_2) is one of the major processes in the production of tropospheric ozone (O_3). Because CO has a longer lifetime than that of most non-methane hydrocarbons (NMHCs), the relative importance of CO for photochemical ozone production is greater in the remote atmosphere. The oxidation of CO by OH represents the major sink for OH (30-60% of OH loss [*Spivakovsky et al*., 2000]) and consequently plays an essential role in controlling the partitioning between OH and the hydroperoxy (HO_2) radical.

Surface CO concentrations have been closely monitored globally since 1988 by the NOAA Climate Monitoring and Diagnostics Laboratory (CMDL) [e.g., *Novelli et al*., 2003, 1998]. In addition to these surface measurements, a relatively long-time record of CO column abundances since around 1995 has been obtained by ground-based Fourier transform IR (FTIR) solar spectrum measurements, and the seasonal and year-to-year variations of CO have been reported [e.g., *Rinsland et al*., 2000, 2002; *Zhao et al*., 2002; *Yurganov et al*., 2005]. FTIR measurement is a spectroscopic technique that can semi-continuously provide information on the vertically averaged CO abundance, including that in the free troposphere, although it can provide only little information on the vertical distribution of CO.

Measurements of CO were made using ground-based FTIR spectrometers at two observatories in Japan (Figure 1): Moshiri Observatory (44.4°N, 142.3°E, 280 m above sea level) and Rikubetsu Observatory (43.5°N, 143.8°E, 370 m above sea level). These two observatories are located at similar latitudes in the northern part of Japan, separated by a distance of 150 km. In this paper, we present seasonal and day-to-day variations of CO in these data during 2001. We compare in situ surface CO measurements at Rishiri Island Observatory (45.1°N, 141.1°E) with the FTIR measurements to confirm the consistency between the measurements. We use a global 3-D chemistry transport model (GEOS-CHEM) to interpret the FTIR CO data. First, we evaluate the model with the FTIR observations. We then use model source-labeled CO tracers, representing contributions from different sources originating from different geographic regions, to investigate how different sources affect the CO abundances at the observation sites.

2. FTIR Measurements

Measurements of CO at Moshiri and Rikubetsu were described in detail by *Zhao et al.* [1997, 2002], and only brief descriptions are given here. High-resolution solar spectra were recorded using ground-based FTIR spectrometers at both sites. We use a Bruker IFS 120HR, with a 450-cm optical path difference (OPD, or spectral resolution of 0.002 cm^{-1}, where the resolution is defined here as 0.9/OPD) and an IFS 120M with a 257-cm OPD (0.0035 cm^{-1}) at Moshiri and Rikubetsu, respectively. To improve the signal-to-noise ratio of Fourier transformed spectra, we only used information with an OPD within 50-cm (0.02 cm^{-1}) for the analyses described below. Measurements at Rikubetsu and Moshiri observatories started in 1995 and 1996 respectively, however only data obtained in the year 2001 are used in this study.

Infrared solar spectra were analyzed using the SFIT2 algorithm, which was jointly developed at the NASA Langley Research Center and the National Institute of Water and Atmosphere Research (NIWA) at Lauder, New Zealand [e.g., *Rinsland et al.*, 2000]. Using this algorithm, a vertical profile of CO is retrieved by fitting the absorption in one or more microwindows (Table 1) in one or more infrared solar spectra. Note that in this study, the microwindow containing the strong CO R(3) line was not used, as various simulation tests indicated that including this window induced a non-linear response (i.e., high CO columns were underestimated) to the expected seasonal range of CO columns. The microwindow covering the range from 2112.08 to 2112.18 cm^{-1}, which contains an isolated solar CO absorption line, was included to accurately capture solar CO absorption features that overlap all terrestrial CO lines. Spectral parameters for the retrieval analyses were taken from the 2000 HITRAN compilation [*Rothman et al.*, 2003].

For the initial vertical profile of CO used in the iterative retrieval analyses, we use a single profile at both sites based on an average of profiles obtained by in situ aircraft measurements during PEM-West A and B [*Zhao et al.*, 1997, Figure 2]. This is because the retrieved profile depends on the initial profile to some extent when the optimal estimation technique is used, and a use of different profiles for different months can distort the seasonal variation of CO. Daily pressure-temperature-altitude profiles at Moshiri-Rikubetsu were constructed using rawinsonde data obtained four times a day at Sapporo (44.1°N, 141.3°E). For altitudes above the balloon sounding height, the 1976 US Standard Atmosphere was smoothly connected to the balloon meteorological data.

In this study, partial column amounts of CO (molecules cm^{-2}) for the 0-4- and 0-12-km altitude ranges were retrieved (strictly speaking, column amounts above 0.28 and 0.37 km for Moshiri and Rikubetsu, respectively). We used averaged mixing ratios of CO (x_{CO}) for these two altitude ranges, which are defined as follows.

$$x_{CO} = N_{CO} / N_{air}$$

where N_{CO} and N_{air} are the partial column amounts of CO and air molecules (molecules cm^{-2}), respectively. Averaging kernels for these retrievals for a typical vertical CO profile (in units of mixing ratio) are shown for solar zenith angles (SZAs) of 30° and 70° in Figure 2. It can be seen that retrievals for layers thinner than 4-km do not provide additional information given the thickness of the averaging kernel. The degrees of freedom (DOF) for the signal was calculated to be 1.98 for a SZA of 70° for typical atmospheric conditions, indicating that in principle CO amounts in two altitude ranges can be independently derived.

Error analyses for these retrievals were made by examining factors listed by *Zhao et al.* [2002], and the results are given in Table 2. The greatest systematic error for the 0-4-km retrievals of 20% results from the a priori profile assumed in this study. This result indicates that the absolute values of retrieved CO amounts for the 0-12-km range are more robust than those of the 0-4-km retrievals. However, considering the DOF of 1.98, the 0-4-km retrievals provide useful information for the partitioning of the tropospheric CO column amounts between two altitude ranges, below and above 4 km. In this study, we present averaged mixing ratios for both 0-4- and 0-12-km altitude ranges.

In the year 2001, CO data are available on 76 and 63 days for Moshiri and Rikubetsu observatories, respectively, with 25 same-day measurements. In general, 1 to 5 spectra were recorded each day when measurements were made, and daily averages of retrieved CO amounts are used in this study. One standard deviation of the retrieved values within a day is 15% or less.

In addition to CO, we also measured and retrieved hydrogen cyanide (HCN) column amounts. HCN is used as an atmospheric tracer of biomass burning in this study, because simultaneous enhancements of FTIR-derived CO and HCN column amounts likely due to influences from biomass burning have been reported [*Zhao et al.*, 2000, 2002]. Corresponding retrieval analyses are described by *Zhao et al.* [2000, 2002]. In this study we have added two extra microwindows: 3268.18 to 3268.27 cm^{-1} and 3299.46 to 3299.58 cm^{-1}, which contain isolated transitions of the HCN υ_3 P(14) and P(4) lines, respectively. The addition of these two microwindows improves the DOF for the signal to about 2, consistent with the CO retrieval.

3. Model Calculations

To evaluate the contributions of various CO sources to CO levels observed in

Japan, the GEOS-CHEM global 3-D chemical transport model (CTM) is used. The version, which we use does not include full-chemistry, but includes simplified chemistry that is enough to simulate CO as detailed below. The GEOS-CHEM CO simulation has previously been applied in a number of studies including the NASA TRACE-P aircraft mission conducted in spring 2001, demonstrating a good simulation of Asian outflow in terms of emissions of CO and precursor gases and transport processes [*Palmer et al*., 2003; *Liu et al*., 2003; *Heald et al*., 2003; *Heald et al*., 2004; *Liang et al*., 2004]. Detailed descriptions of the model are given elsewhere by *Palmer et al*. [2003]. Briefly, the model version used here has a horizontal resolution of 2° latitude x 2.5° longitude and has 48 vertical levels, 20 of which are below 12 km. The model is driven by assimilated meteorology from the Goddard Earth Observing System (GEOS) of the NASA Data Assimilation Office.

We use gridded emission inventories for anthropogenic fossil fuel and biofuel burning in East Asia from *Streets et al*. [2003]. Because previous inversion studies suggest that anthropogenic CO emissions from China are likely to have been underestimated [*Palmer et al*., 2003; *Carmichael et al*., 2003; *Heald et al*., 2004; *Arellano et al*., 2004; *Wang et al*., 2004], anthropogenic emissions from China are increased by 54% to account for this discrepancy [*Palmer et al*., 2003; *Heald et al*., 2004]. *Streets et al*. [2003] showed that there is a small seasonal variation of Chinese anthropogenic CO emissions due to residential fuel use, but we use annually averaged emissions in this study. Fossil fuel and biofuel emissions for the rest of the world are taken from *Duncan et al*. (manuscript in preparation, 2005) and *Yevich and Logan* [2003], respectively. We use a climatological biomass burning inventory developed by J. A. Logan, representative of data taken between 1980 and the early 1990s [*Lobert et al*., 1999]. These emissions are distributed seasonally using a climatology developed by *Duncan et al*. [2003] that uses data from the Along Track Scanning Radiometer (ATSR, 1996-2000) and Advanced Very High Resolution Radiometer

(AVHRR, 1992-1994) satellite instruments. The activity in 2001 in northern Asia and eastern Russia (45°-70°N and 80°-180°E) estimated using ATSR satellite data was found to be close to the average activity over years between 1996 and 2004 (private communication: Dr. Fok-Yan Leung, Harvard University, 2005). We include indirect emissions of CO from the oxidation of anthropogenic VOCs co-emitted with CO by increasing direct emissions by 20% (fossil fuel) and 10% (biofuel and biomass burning). These scaling factors were derived from non-methane volatile organic compound (NMVOC) emissions from fossil fuels [*Piccot et al.*, 1992] and biofuel burning [*Yevich and Logan*, 2003], emission factors for individual NMVOCs [*Andreae and Merlet*, 2001], and molar yields of CO from individual NMVOCs [*Altshuller*, 1991].

There is also a large photochemical source of CO from the oxidation of methane (CH_4) and biogenic NMVOCs, which is treated following the approach of Duncan et al. (manuscript in preparation, 2005). The source of CO from the oxidation of CH_4 is calculated from a global 3-D distribution of CH_4 based on observations and a global 3-D distribution of OH calculated using a full-chemistry version of GEOS-CHEM (v4.33). We use a molar yield of CO of unity for CH_4 oxidation, leading to a global CO production rate of 850 Tg CO/yr. For the source of CO from oxidation of biogenic NMVOCs, we take monthly mean emissions from previous studies [*Guenther et al.*, 1995; *Wang et al.*, 1998; *Singh et al.*, 2000; *Jacob et al.*, 2002] and scale them with the molar yields of CO of *Altshuller* [1991]. These emissions are emitted directly as CO in the model calculations. This work is described further by Duncan et al. (manuscript in preparation, 2005). The resulting emission rates in terms of CO for isoprene, methanol, monoterpenes, and acetone are 175, 85, 70, and 25 Tg CO/yr, respectively. To calculate the loss of CO, we use global 3-D monthly mean OH concentration fields calculated from a full-chemistry GEOS-CHEM simulation (v4.33).

To study contributions of various CO sources to the CO levels observed in

Japan, we conducted a “source-labeled” (or “source-tagged”) CO simulation [*Palmer et al*., 2003; *Liang et al*., 2004]. In this simulation, total CO is expressed as a linear sum of contributions from fossil and bio- fuel burning (FF) and biomass burning (BB) from individual geographic regions (Figure 1a). These individual contributions are tracked and will be used to interpret variations in the FTIR CO observations. For FF CO, emissions in Asia, Europe, North America, and other regions are resolved. For BB CO, emissions in Asia, Africa, South America, and other regions are resolved. In addition, photochemically produced CO is labeled. Because the major photochemical CO production is the oxidation of CH_4, this CO source is diffuse over the globe.

Model CO concentrations were saved every hour at each site. We use daytime averages (0600 to 1800 solar local time) for the present analyses. Model vertical profiles are scaled by the averaging kernel of the FTIR measurements (Figure 2) to account for the vertical resolution of the measurements, as follows:

$$\tilde{x} = (A - I)x_0 + Ax,$$

where x_0 is a vector of the initial vertical profile of CO used for the FTIR retrieval analyses, x is a vector of model-calculated values, $\tilde{x}$ is a vector of averaged values to be compared with observations, A is the averaging kernel matrix, and I is a unit matrix. Because the vertical shape of an averaging kernel changes with SZA (Figure 2), the SZA at which measurements had been made was averaged for individual days and an averaging kernel for this averaged SZA was used for each day.

4. Results

4.1. Comparison of the Two FTIR Measurements

Measurements of CO were made at both Moshiri and Rikubetsu on the same day on 25 total days in 2001. In Figure 3a, a scatter plot between the CO values observed at these two sites (0-4-km retrieval) is shown. In general, these two measurements agreed to within a root-mean-square (RMS) difference of 12 parts per billion by volume (ppbv) or 7.2%, with an r^2 value of 0.75. A linear fit to the data (orthogonal regression) results in a slope of 1.04 with a small intercept (-2.1 ppbv). The agreement between the two measurements indicates that the overall errors in the measurements are within the estimated uncertainties, confirming the validity of the measurements. The agreement also indicates that CO observations at these sites are not affected by local CO sources, and results can be considered to represent CO values in northern Japan over an area with a horizontal scale of over 150 km, the distance between the two observatories. Considering the spatial resolution of the GEOS-CHEM model of 2° x 2.5°, this result indicates that it is reasonable to make a direct comparison between the measurements and model calculations. In the following analyses, we combined the Moshiri and Rikubetsu data and refer to them as Moshiri-Rikubetsu data hereafter; if only one of the two data sets is available, it is used, and if both data sets are available, an average is taken. As a result, the set of available data increases to a total of 114 days.

FTIR-derived CO values at Moshiri are also compared with in situ surface measurements made at Rishiri Island Observatory (Figure 1), which is located 130 km north of the Moshiri observatory (Figure 3b). In situ CO measurements were made using a modified non-dispersive infrared (NDIR) photometer instrument (Kimoto, model 541) [*Tanimoto et al.*, 2002a]. For cases in which in situ CO concentrations are lower than 200 ppbv, no apparent systematic bias is found between the measurements (a slope of 0.94 with an intercept of -3.6 ppbv). This result further confirms the validity of the FTIR measurements and retrieval for the 0-4-km altitude range. This result also suggests that the CO partial column for the 0-4-km retrieval generally shows similar behavior to that of surface CO. When CO concentrations are greater than 200 ppbv, CO values at the surface are systematically higher than the FTIR 0-4-km retrieval values, which is likely due to greater enhancement of CO near the surface.

4.2. Seasonal Variation

In Figure 4, a time series of daily 0-4-km CO mean mixing ratio values from the Moshiri-Rikubetsu retrieval is shown. Monthly averages of 0-4 and 0-12 km are also shown in Figure 5 and given in Table 3. As also listed in Table 3, 7 to 16 daily data are available for individual months. As seen in these figures and table, a seasonal maximum and minimum appear in spring (April) and early fall (September), respectively. The monthly averages in April and September for the 0-4-km retrievals are 192 and 136 ppbv, respectively. The seasonal variation of tropospheric CO, with its maximum in winter/early spring and minimum in summer, is observed over the globe [e.g., *Novelli et al.*, 1992, 1998; *Rinsland et al.*, 2000, 2002; *Zhao et al.*, 2002]. It is largely driven by the seasonal variation in OH concentration; smaller OH concentrations and hence a longer lifetime of CO during winter result in an accumulation of CO toward spring until loss by OH surpasses inputs of CO (emissions and photochemical production). Seasonal variations of emission strength and transport also cause seasonal variations in the CO concentrations depending on the location of the measurements. Surface CO measurements made by NOAA/CMDL indicate that the maximum and minimum northern hemispheric averaged CO concentrations appear in March and July, respectively [*Novelli et al.*, 1998]. Compared with these results, the seasonal minimum appears slightly later (September) at Moshiri-Rikubetsu. A seasonal minimum around September was also observed by ground surface measurements at Rishiri Island [*Tanimoto et al.*, 2002b]. As discussed later in section

5.1, changes in both photochemistry and transport pattern cause the observed seasonal minimum in northern Japan.

In Figure 6, the ratio of partial column amounts between the 0-4-km and 0-12-km altitude ranges is shown. There is a seasonal variation with a peak-to-peak amplitude of 10%, although about 3% is due to the change in air density. A seasonal maximum and minimum appear in February-March and August, respectively, indicating that a seasonal increase in CO in the lower troposphere is slightly greater compared to that in the middle-upper troposphere in late-winter/early-spring, while the contrast in CO mixing ratio between the lower and upper altitudes becomes smaller in late summer. Because the DOF is nearly 2 (SZA = 70°) for the FTIR retrievals in this study, it is possible to derive the seasonal tendency in the vertical structure of the CO profile, although the vertical resolution of the FTIR measurements and retrieval analyses is limited. During summer a vertical gradient in the CO profile is expected to diminish through vertical mixing, while during winter a vertical change in anthropogenic influences results in vertical gradients in the CO profile, as will be discussed later in more detail in section 4.5.

Although discussion of the year-to-year variation is outside the scope of this paper, we note here that 2001 appears to exhibit a typical seasonal variation, based on the 1995-2000 time series of FTIR-derived CO partial columns from Moshiri-Rikubetsu [*Zhao et al.*, 2002]. This time series showed that a regular seasonal variation was observed except for the year 1998, when a significant increase, likely due to influences from biomass burning over eastern Siberia, was observed. The monthly averaged CO values (both 0-4 and 0-12 km) observed in 2001 are generally in the range of the standard deviation of daily values within individual months observed in the years 1996, 1997, 1999, and 2000.

4.3. Comparison with GEOS-CHEM Model

Model-calculated CO amounts (daily and monthly) are compared with Moshiri-Rikubetsu observations in Figures 4 and 5. As described in section 2, model-calculated values were smoothed using averaging kernels from the FTIR retrieval analyses so that direct comparison with observations can be made. To calculate monthly averages, only model results on days when observation data are available (which are shown in Figure 4) are used. As seen in these figures, the GEOS-CHEM model generally reproduces the observed seasonal variations. The RMS differences between the daily values and the monthly averages for the 0-4-km retrievals are 22 ppbv (14%) and 17 ppbv (11%), respectively, which is within the combined uncertainties in the absolute value of the observations and model calculations. The r^2 values for the monthly averages are 0.80 (0-4 km) and 0.78 (0-12 km). An underestimation by the model is found between March and June for both the 0-4- and 0-12-km altitude ranges. For the 0-4-km range, the model underestimates the observations by 21-27 ppbv or 12-14% during this time period. One of the possible explanations for this difference is an underestimation of the BB contribution in the model, as discussed later in section 5.3.

In Figure 6, the model-calculated partial column ratio between the 0-4-km and 0-12-km altitude ranges is compared with observations. In general, a good agreement in absolute value and its seasonal variation is found, although the vertical gradient was slightly overestimated in summer. These results suggest that the model calculation successfully reproduced the processes driving the seasonal variation in the vertical structure of the CO profile.

Finally, day-to-day variations are compared (Figure 7). To eliminate the correlation caused by the seasonal variations, a monthly average is subtracted from individual daily values and residual values are compared. As a result, it is found that the model calculation reproduced the observed day-to-day variation to some extent with an r^2 value of 0.23. It is also seen in the time series plot (Figure 4) that the model captured pronounced increases, for example, on days 100, 145, 169, and 218-219, with lower values around each event. Considering the lifetime of CO ranges from a few weeks to several months, the agreement in the day-to-day variation indicates that the transport process and the emission inventory in the model are generally good.

The agreement with CO observations in absolute value, seasonal variations, day-to-day variations, and in the ratio of partial column amounts between the 0-4- and 0-12-km altitude ranges confirm the validity of the model calculations. In the following sections, results from the "source-labeled" CO simulations are presented, and processes that contribute to these observed variations are discussed.

4.4. Individual Source Contributions

In this section, results from "source-labeled" CO simulations for Moshiri and Rikubetsu observatories are presented, and contributions from different CO sources originating from different geographic locations (Figure 1a) are described. In Figure 8, a time series of model-calculated daily CO values is shown at a sigma level of 0.90 (altitude of about 1 km), where the sigma level is defined as follows:

$$\sigma = \frac{p - p_T}{p_S - p_T},$$

where p is atmospheric pressure at the level at which CO concentrations are calculated in the model, p_S is atmospheric pressure at the surface, and p_T is atmospheric pressure at the top boundary of the model (0.001 hPa in this calculation). In Figure 8, various source contributions (results from "source-labeled" simulations) are also shown. For this plot, results for all days in the year 2001 are shown, irrespective of the date of observation. In Figure 9, monthly averages are shown. When yearly averaged contributions at 1 km are examined (Table 4), the contributions from Asian FF combustion and photochemical production are the greatest (31% each). Contributions from European FF combustion (18%) and that from North American FF combustion

(9%) follow.

As seen in Figures 8 and 9, seasonal variation in the modeled CO is caused by a complex interaction between various CO source contributions. The contribution from Asian FF combustion (AS_FF) increases from January to July (38 to 72 ppbv) and is greatest between May and July. Its contribution suddenly decreases between July and August by a factor of about 2 (72 to 34 ppbv), and it stays relatively constant for the rest of the year. These seasonal changes can generally be interpreted as changes in the origin of transported air parcels caused by seasonal variation in the meteorological fields over East Asia, as discussed later in section 5.1. It is evident that most of the day-to-day variations in total CO values are due to Asian FF combustion. This is presumably because CO emission sources are close to the observatories and air parcels influenced by these emission sources are transported to the observatories without significant dilution. Consequently, day-to-day variation of transport processes directly cause day-to-day variations of CO concentrations.

Contributions from European and North American FF combustion (EU_FF and NA_FF) are large between October and April, with a maximum contribution appearing around January at an altitude of 1 km. During winter months, the European contribution is comparable to that from Asian FF combustion, indicating that inter-continental long-range transport, due to the longer CO lifetime and favorable wind patterns (section 5.2), maintains the observed high CO levels over northern Japan.

The contribution from biomass burning in Asia (AS_BB) is generally large between April and September. As noted above, a climatological source distribution and strength were used for this calculation. The yearly averaged contribution is 6%. The contributions from biomass burning in Africa and South America were found to be less than 2%.

The contribution from photochemical CO production (Chemical) from oxidation of methane and NMVOCs has a comparable yearly averaged contribution

(31%) to that of Asian FF combustion at an altitude of 1 km, as described above. Oxidation of CH_4 by OH is the dominant pathway of photochemical production of CO, and short-lived biogenic NMVOCs make only small contributions. Between August and December, the contribution from photochemical CO production is greatest within the CO sources considered in this study. In August and September especially, this contribution is dominant (44 and 49%, respectively, of the total CO). When the absolute amount of the photochemical contribution is examined, the greatest contribution appears in July-August, in accordance with the highest photochemical activities, while the minimum contribution appears in April. It is noted that the contribution is 40-60 ppbv throughout the year (or ±17% change from the average), and it does not necessarily decrease significantly during winter, in spite of a more-than-a-factor-of-20 reduction in OH concentration near the surface at mid-latitudes (e.g., 0.9 and 23.1 x 10^5 molecules cm^{-3} in January and July, respectively, at 900 hPa and 44°N [*Spivakovsky et al.*, 2000]). This is likely because both photochemical production and loss are smaller in winter than in summer. Although the chemical production rate of CO is low in winter at high latitudes, CO continues to accumulate because of the long lifetime of CO (low OH radical levels).

4.5. Vertical Profiles of Individual Source Contributions

Vertical profiles of various source contributions at Moshiri-Rikubetsu are shown in Figures 10a and 10b for January and July, respectively. As seen in these figures, contributions from various sources have different vertical structure and seasonal variations. Here we examine these features for individual sources.

A contribution from Asian FF combustion (AS_FF) decreased remarkably with altitude from surface to 4 km (630 hPa) during summer. Because GEOS-CHEM overestimates surface CO values obtained by in situ measurements at Rishiri in summer months (a monthly average of observed CO in July is 145 ± 37 ppbv), the vertical mixing near the surface could be underestimated by the model, and the vertical gradient could be overestimated. These large vertical changes in spring and summer months in the model results were likely due to influences from horizontal transport of CO within the boundary layer from sources in Japan and neighboring countries (see discussion about transport pathway for summer months in section 5.1.). In the free troposphere, a less pronounced vertical gradient is found both in July and January for the Asian FF combustion contribution.

A contribution from European FF combustion (EU_FF) decreases with altitude throughout the troposphere in January (46 and 18 ppbv at 1 and 6 km or 900 and 460 hPa, respectively). The absolute value of the reduction in this altitude range is greater than those of the other CO sources and accounts for 60% of the reduction of CO amount at this altitude range (Asian FF contribution accounts for 23%). As a consequence, the vertical gradient of the CO profile in January is primarily due to the vertical gradient of the European FF contribution (Figure 10a). As described above in section 4.2, a seasonal maximum of the partial column ratio of CO between 0-4 and 0-12 km appears in February-March in both observations and model calculations (Figure 6), suggesting that the vertical gradient of CO concentration is greatest in late-winter/early-spring. The results presented in this study suggest that the most important driver to make this seasonal maximum is the inter-continental transport of European FF CO. During summer, the contribution is much smaller, especially within the boundary layer, and the maximum contribution appears in the free troposphere (around 5 km or 550 hPa, Figure 10b). The very small contribution in the boundary layer in summer is because meteorological conditions are not favorable for direct transport of European air parcels to Japan (section 5.2.) and because the photochemical lifetime of CO is short near the surface

The contribution of photochemical production (Chemical) of CO shows only a small decrease with altitude both in summer and winter (20-30% reduction from the surface to the tropopause). The lack of vertical dependence was likely because both production and loss rates are larger at lower altitudes. A small seasonal variation in the photochemical contribution is likely because both production and loss rates are large in summer, as described in the previous section.

5. Discussion

5.1. Transport Pathways and Influence from Asian Fossil Fuel Combustion

In Figures 11a and 11b, the mean wind field at 925 hPa (≈1 km) is shown for January and July. In Figures 12a and 12b, 10-day kinematic back trajectories [Tomikawa and Sato, 2005] starting from over Moshiri at an altitude of 1 km are shown (one trajectory for each day). Color coding shows the atmospheric pressure of air parcels along the trajectories. For this calculation, meteorological data provided by the European Centre for Medium-Range Weather Forecasts (ECMWF) on a 2.5° × 2.5° latitude-longitude grid were used. The wind fields in the year 2001 are generally similar to the 25-year averages of years between 1980 and 2004, although the easterly component of the wind field over the Sea of Okhotsk and the westerly component over the Sea of Japan in January and July, respectively, are greater in 2001. As seen in these figures, in January, northerly monsoonal winds between the Siberian high and Aleutian low dominated over northern Japan. As a result, air over far-east Siberia was generally transported to the Moshiri-Rikubetsu region, and some direct transport from the north of Europe within 10 days is also seen. In July, southwesterly winds are seen over the Moshiri-Rikubetsu region, and the wind speed is generally lower than that in January. As a result, air masses arriving at low altitudes generally had stagnated around Japan and the Japan Sea, so that they received emissions over Japan and the eastern rim of the Asian continent. Note that there is a relatively large uncertainty in the individual trajectory calculations for air parcels arriving at 1 km due to vertical mixing of air within the planetary boundary layer. However, the general features of the trajectories in each season are considered to be captured by these calculations.

To study the locations of emission sources that could have affected air parcels arriving at the Moshiri-Rikubetsu region in more detail, CO emissions that individual air parcels received along trajectories were integrated at each emission grid box (Figures 13a and 13b). In this calculation, the total time duration in which individual air parcels existed in each grid box at altitudes below the 800-hPa level was calculated and it was multiplied by the CO emissions for this particular grid. The emission inventory provided by *Streets et al*. [2003] increased by a factor of 1.54 (see description in section 3) was used for East Asia. The EDGAR 1995 emission inventory [*Olivier et al*., 2001; http://arch.rivm.nl/env/int/coredata/edgar/] was used for the rest of the world because of its high spatial resolution (1° x 1° in latitude and longitude). Because the absolute amount of calculated values does not have physical meaning, arbitrary units are chosen for these figures to show relative source contributions from various regions. As seen in these figures, in January, emissions from the east rim region of the Asian continent facing the Rikubetsu-Moshiri region contributed to the increase of the CO level in addition to emissions within northern Japan. In contrast, in July, emission sources over a wide region in Japan, the Korean Peninsula, and the northeastern part of China contributed to the CO abundance in northern Japan. This seasonal change in the locations of the dominant source regions was due to a shift of wind direction from northerly to southwesterly, as described above (Figures 11a and 11b). This wind regime shift caused a greater contribution of Asian fossil fuel combustion CO sources in July as compared with that in January at 1 km, as already described in section 4.4 (Figure 9). When the seasonal variation of wind regime from winter to summer is examined month by month, the mean wind direction is found to change from northerly (winter) to westerly (spring) and to southwesterly (summer), causing a gradual increase in Asian fossil fuel contributions.

In August, the mean wind at 925 hPa weakened and shifted to the southeasterly direction, which brought cleaner maritime air to the Moshiri-Rikubetsu region (not shown), resulting in a factor-of-2 reduction in Asian FF contributions from July to August (Figure 9), as described in section 4.4. Between September and December, the wind direction at 925 hPa changed to westerly and then to northwesterly while increasing in speed. A slightly higher Asian FF contribution in October and November than in previous and subsequent months (Figure 9) resulted from transport of anthropogenic CO by the westerlies that appeared in these two months.

As described in section 4.2, a seasonal minimum of CO in northern Japan appears slightly later than the northern hemispheric average (September versus July) derived from NOAA/CMDL surface CO measurements [*Novelli et al.*, 1998]. As shown above, July is the month when the influence from Asian FF combustion is quite large, because of southwesterly winds. In August and September, cleaner air is transported to northern Japan, resulting in a seasonal minimum. Meteorological conditions, in addition to photochemistry, likely cause the difference in seasonal variation.

5.2. Influence from European Fossil Fuel Combustion

European FF contributions are comparable to those of Asian FF contributions in winter months at Moshiri-Rikubetsu at 1 km (Figure 9). The contributions decrease with increasing altitude with a factor-of-2.5 reduction between 1 and 6 km in January (Figure 10a). This vertical gradient of European FF contributions resulted in a vertical gradient in the CO profile in winter, and this process was likely responsible for the observed seasonal maximum of the partial column ratio of CO between 0-4 and 0-12 km in February-March (see Figure 6 and description in section 4.5). The large contribution in the winter lower troposphere is considered to be due to the following two factors. First, because of the long chemical lifetime of CO at high latitudes during winter, CO emitted into the atmosphere accumulated, resulting in the inter-continental impact. Emitted CO could have circulated the globe at northern high latitudes by the circumpolar westerlies before arriving at the Moshiri-Rikubetsu region. Weak vertical transport processes during the winter caused higher European FF contributions at lower altitudes. Second, clockwise circulation around the Siberian high caused direct transport of air parcels influenced by European CO sources to the Moshiri-Rikubetsu region. This airflow can be seen in trajectories of air parcels arriving at Moshiri-Rikubetsu (Figure 12a). The descending motion of air through the northerly monsoonal flow between the Siberian high and Aleutian low resulted in higher contributions from European fossil fuel combustion at lower altitudes, resulting in the vertical gradient in the contributions shown in Figure 10a. The direct transport process can be identified in the relatively large day-to-day variation of European fossil fuel contributions as compared with that of North American FF contributions shown in Figure 8 (EU_FF and NA_FF). In other words, the transport process is an episodic event, which can take place when the meteorological fields are favorable. The very small day-to-day variation of North American FF contributions indicates that direct transport is small and the contributions are likely due to accumulation at high latitudes as described above. Considering a small vertical gradient of the North American FF contributions, direct transport of European FF CO (the second process described above) could be more important for making the vertical gradient of the European FF contribution.

The fossil fuel contributions both from Europe and North America are smaller between May and September as compared with those in the rest of the year at 1 km altitude (Figure 9). The smaller contributions are again consistent with the shift in the wind regime near the surface (southerly wind during later summer and early fall) and shorter photochemical lifetime of CO. When the vertical profile of contributions from European fossil fuel combustion is examined for July conditions (Figure 10b), the maximum is found in the free troposphere (around 5 km), although its absolute values are much smaller than those in January (Figure 10a). Although southwesterly wind is seen near the surface, westerly winds dominate in the free troposphere, which brings air parcels influenced by European sources (not shown).

5.3. Possible Influences from Boreal Forest Fire

The model calculations underestimate CO amounts between March and June by 21-27 ppbv (12-14%) (Figure 5). Anthropogenic emissions in northern Asia and eastern Russia could be underestimated in our calculations, although this hypothesis has some difficulty explaining the seasonality of the underestimation. Another possible explanation is an underestimation of BB contributions such as those from far-east Russia. Although the fire counts in 2001 in northern Asia and eastern Russia (45°-70°N and 80°-180°E) obtained by the ATSR satellite were close to average, it is worthwhile examining this hypothesis considering the uncertainty in our estimation of BB activities.

In Figure 14, hot spots detected by ATSR satellite measurements [*Stricker et al.*, 1995] are shown for April 2001 with back trajectories of the air parcels arriving at Moshiri at 1 km altitude. As seen in this figure, there were some BB activities in far-east Russia in the region centered around 50°N and 125°E, which could influence CO levels in northern Japan. Although the number of hot spots in this region is greater in July-August, as for intensive forest fire events in 1998 [*Kajii et al.*, 2002; *Zhao et al.*, 2002], the impact on Moshiri-Rikubetsu CO can still be large in earlier months in 2001, considering trajectories of air parcels sampled at these sites (Figures 12a and 12b).

In this study, we also examined the relationship between the CO and HCN amounts derived from FTIR measurements, because HCN is produced by BB in addition to anthropogenic combustion (likely due to residential coal burning), especially in China [e.g., *Li* et al., 2000, 2003; *Singh et al.*, 2003]. In Figure 15, a scatter plot between daily values of CO and HCN (0-12-km retrievals) is shown for months when influence from far-east Russian BB activity can be expected. *Zhao et al.* [2002] reported clear simultaneous enhancements of FTIR-derived CO and HCN column amounts observed at Moshiri-Rikubetsu in 1998, which were quite likely due to influences from BB over far-east Russia. We also observed simultaneous enhancements in 2002, when boreal forest fire activities in Russia were intense [*Yurganov et al.*, 2005]. A ratio of enhancements (daily anomalies from the normal seasonal variation) between HCN and CO (ΔHCN/ΔCO) is calculated using the method described by *Zhao et al.* [2002] to find a good agreement in ratios between the two events observed in 1998 and 2002 (1.28 and 1.27 parts per trillion by volume (pptv)/ppbv). In Figure 15, a line having this slope is shown as a solid line. On the other hand, it is difficult to estimate ΔHCN/ΔCO ratios in air parcels influenced by residential coal burning in China because HCN and CO values in the low-BB-activity season (between November and February in 1996-1997, 1999-2000, and 2000-2001) do not show a clear correlation (not shown). This can be partly because of smaller Asian FF contributions in these months. Based on in situ measurements during TRACE-P, *Singh et al.* [2003] and *Li et al.* [2003] reported that ΔHCN/ΔCO ratios are systematically lower in Chinese urban plumes (likely due to residential coal burning) than in BB plumes (1.3-1.7 and 2.7-3.4 pptv/ppbv, respectively). Although these ratios cannot be directly compared with FTIR measurements because of differences in the vertical profile of the averaging kernels between HCN and CO measurements, a similar tendency can be expected for the column amount ratios. The FTIR-derived ΔHCN/ΔCO ratios between March and May 2001 (a slope for individual month data) are generally similar to or greater than the ratios influenced by BB activities in 1998 and 2002 (Figure 15). Although we could not evaluate influences from coal burning on observed ΔHCN/ΔCO ratios, the present results are consistent with some BB influences in spring 2001. Because of a relatively small contribution from Asian BB of 7-11% (including BB in far-east Russia, see Figure 1) for the time period when the model underestimates the observations (March-June), BB activities in far-east Russia or other regions could have contributed more to the observed CO levels than those in the model calculations. To quantify the BB source strength more accurately, further investigations performing multi-year model calculations should be done.

6. Conclusions

Tropospheric CO measurements were made throughout 2001 using ground-based FTIR spectrometers at Moshiri (44.4°N, 142.3°E) and Rikubetsu observatories (43.5°N, 143.8°E) in northern Japan, which are separated by 150 km. CO amounts at altitude ranges of 0-4 and 0-12 km were retrieved using the vertical profile retrieval algorithm SFIT2. Retrieved CO amounts in the 0-4-km layer obtained at the two observatories agreed within uncertainties, indicating that observed CO values were not affected by local sources and can be considered to represent CO levels in northern Japan. Reasonable agreement was also found between the 0-4-km retrieved values and in situ CO measurements, except for pollution transport events (surface CO > 200 ppbv), providing further support corroborating the FTIR measurements.

Seasonal maximum and minimum FTIR-derived tropospheric CO amounts occurred in April and September, respectively (192 and 136 ppbv for the 0-4-km retrieval). The ratio of partial column amounts between the 0-4- and 0-12-km altitude ranges was found to be slightly greater in early spring. The GEOS-CHEM model calculations generally reproduced these observed features, although model calculations underestimated observations between March and June.

Contributions from various CO sources, such as anthropogenic FF combustion, BB, and photochemical production from CH_4 and NMVOCs were evaluated using source-labeled CO model calculations. The results presented in this study show that the observed seasonal variation was caused by a combination of seasonal variations of various source contributions in addition to a seasonal change in CO loss by reaction with OH. The contribution from Asian FF combustion increased from January to July, and it decreased by a factor of about 2 between July and August, staying relatively constant for the rest of the year. Trajectory analysis of observed air parcels indicated that a seasonal change in the meteorological fields largely controlled the changes in these contributions. Weak southwesterly winds during summer brought more Asian pollution to Moshiri-Rikubetsu than in other seasons. Most of the day-to-day variations in CO values were also found to be due to those of the Asian FF contributions.

The inter-continental transport of European FF combustion CO was found to be comparable to Asian FF sources in winter at 1 km altitude. In this season, northwesterly winds around the Siberian high brought pollutants from Europe directly to Japan, in addition to southward transport of accumulated pollution from higher latitudes. The influences were generally greater at lower altitudes because of the descending motion of air. This vertical gradient of European FF contributions resulted in a vertical gradient in the CO profile in winter, and this process was likely responsible for the observed seasonal maximum of the partial column ratio of CO between 0-4 and 0-12 km in February-March. The present study demonstrates that source-labeled model calculation is a useful tool for quantitative estimation of inter-continental transport, as also demonstrated in previous studies [e.g., *Liang et al.*, 2004].

The contribution from photochemical CO production from oxidation of CH_4 and NMVOCs was greatest between August and December, among the CO sources considered in this study. When the absolute amount of the photochemical contribution was examined, the greatest contribution appeared in July-August, in accordance with the highest photochemical activities. The seasonal change in the contribution was only ±17% likely because both photochemical production and loss are greater in summer than in winter. The photochemical contribution also had small vertical variations both in summer and winter (20-30% reduction from surface to tropopause), likely because both production and loss rates are larger at lower altitudes.

When the yearly averaged contributions at 1 km were examined, the contribution from Asian FF combustion and photochemical production were the greatest (31% each). The contribution from European FF combustion (18%) and that from North American FF combustion (9%) followed.

Model calculations underestimated CO amounts by 12-14% between March and June. Fire-count data obtained by ATSR satellite measurements and the relationship between FTIR-derived HCN and CO amounts are generally consistent with BB influences in spring; however, a quantitative estimate could not obtained in this study. Because the year-to-year variation of tropospheric CO is largely controlled by BB CO emissions, further study is need to evaluate their impacts on the budget of CO.

Acknowledgements.

The authors would like to thank M. Sera, Y. Ikegami, and H. Hanano for their assistance in the FTIR observations at Moshiri and Rikubetsu. The kind and helpful cooperation of the town of Rikubetsu is also greatly appreciated. The authors wish to acknowledge the public use of the ATSR World Fire Atlas. The meteorological data were supplied by the European Centre for Medium-Range Weather Forecasts (ECMWF). This work was supported in part by the Ministry of Education, Culture, Sports, Science, and Technology (MEXT). The trajectory calculation program used in this paper was developed by Y. Tomikawa and K. Sato at the National Institute of Polar Research, Japan. The work at Harvard was supported by the NASA Atmospheric Chemistry Modeling and Analysis Program.

References

Altshuller, P. (1992), The production of carbon monoxide by the homogeneous NOx-induced photooxidation of volatile organic compounds in the troposphere, *J. Atmos. Chem., 13*, 155-182.

Andreae, M., and P. Merlet (2001), Emission of trace gases and aerosols from biomass burning, *Global Biogeochemical Cycles, 15*, 955-966.

Arellano Jr., A. F., P. S. Kasibhatla, L. Giglio, G. R. van der Werf, and J. T. Randerson (2004), Top-down estimates of global CO sources using MOPITT measurements, *Geophys. Res. Lett., 31*, L01104, doi:10.1029/2003GL018609.

Bey, I., D. J. Jacob, J. A. Logan, and R. M. Yantosca (2001), Asian chemical outflow to the Pacific in spring: Origins, pathways, and budgets, *J. Geophys. Res., 106*, 23,097-23,113.

Bertschi, I. T., and D. A. Jaffe (2005), Long-range transport of ozone, carbon monoxide, and aerosols to the NE Pacific troposphere during the summer of 2003: Observations of smoke plumes from Asian boreal fires, *J. Geophys. Res., 110*, D05303, doi:10.1029/2004JD005135.

Carmichael, et al. (2003), Evaluating regional emission estimates using the TRACE-P observations, *J. Geophys. Res., 108*(D21), 8801, doi:10.1029/2002JD003116, 2003.

Duncan, B. N., R. V. Martin, A. C. Staudt, R. Yevich, and J. A. Logan (2003), Interannual and seasonal variability of biomass burning emissions constrained by satellite observations, *J. Geophys. Res., 108*(D2), 4100, doi:10.1029/2002JD002378.

Guenther, A., et al. (1995), A global model of natural volatile organic compounds emissions, *J. Geophys. Res., 100*, 8873-8892.

Heald, C. L., et al. (2003), Asian outflow and trans-Pacific transport of carbon monoxide and ozone pollution: An integrated satellite, aircraft, and model perspective, *J. Geophys. Res., 108(D24)*, 4804, doi:10.1029/2003JD003507.

Heald, C. L., et al. (2004), Comparative inverse analysis of satellite (MOPITT) and aircraft (TRACE-P) observations to estimate Asian sources of carbon monoxide, *J. Geophys. Res., 109*, D23306, doi:10.1029/2004JD005185.

Holloway, T., H. L. Levy II, and P. Kasibhatla (2000), Global distribution of carbon monoxide, *J. Geophys. Res., 105*, 12,123-12,147.

Intergovernmental Panel on Climate Change (IPCC) (2001), Climate change 2001: The scientific basis, Geneva.

Jacob, D. J., B. D. Field, E. Jin, I. Bey, Q. Li, J. A. Logan, and R. M. Yantosca (2002), Atmospheric budget of acetone, *J. Geophys. Res., 107,* 10.1029/2001JD000694.

Kajii, et al. (2002), Boreal forest fires in Siberia in 1998: Estimation of area burned and emissions of pollutants by advanced very high resolution radiometer satellite data, *J. Geophys. Res., 107(D24)*, 4745, doi:10.1029/2001JD001078.

Li, Q., D. J. Jacob, I. Bey, R. M. Yantosca, Y. Zhao, Y. Kondo, and J. Northolt (2000), Atmospheric hydrogen cyanide (HCN): Biomass burning source, ocean sink?, Geophys. Res. Lett., 27, 357-360.

Li, Q., D. J. Jacob, R. M. Yantosca, C. L. Heald, H. B. Singh, M. Koike, Y. Zhao, G. Sachse, and D. Streets (2003), A global three-dimensional model analysis of the atmospheric budgets of HCN and CH3CN: Constraints from aircraft and ground measurements, *J. Geophys. Res., 108(D21)*, 8827, doi:10.1029/2002JD003075.

Liang, Q., L. Jaegle, D. A. Jaffe, P. Weiss-Penzias, A. Heckman, and J. A. Snow (2004), Long-range transport of Asian pollution to the northeast Pacific: Seasonal variations and transport pathways of carbon monoxide, *J. Geophys. Res., 109*, D23S07, doi:10.1029/2003JD004402.

Liu, H., D. J. Jacob, I. Bey, R. M. Yantosca, B. N. Duncan, and G. W. Sachse (2003), Transport pathways for Asian combustion outflow over the Pacific: Interannual and seasonal variations, *J. Geophys. Res.*, *108*(D20), 8786, doi:10.1029/2002JD003102.

Lobert, J., W. Keen, J. Logan, and R. Yevich (1999), Global chlorine emissions from biomass burning: Reactive chlorine emissions inventory, *J. Geophys. Res., 104*, 8373-8389.

Logan J. A., M. J. Prather, S. C. Wofsy, and M. B. McElroy (1981), Tropospheric chemistry: A global perspective, *J. Geophys. Res., 86*, 7210-7254.

Novelli, P. C., P. Steele, and P. P. Tans (1992), Mixing ratios of carbon monoxide in the troposphere, *J. Geophys. Res., 97*, 20,731-20,750.

Novelli, P. C., K. A. Masarie, and P. M. Lang (1998), Distributions and recent changes of carbon monoxide in the lower troposphere, *J. Geophys. Res., 103*, 19,015-19,033.

Novelli, P. C., K. A. Masarie, P. M. Lang, B. D. Hall., R. C. Myers, and J. W. Elkins (2003), Reanalysis of tropospheric CO trends: Effects of the 1997-1998 wildfires, *J. Geophys. Res., 108*(D15), 4464, doi10.1029/2002JD003031.

Olivier, J.G.. J. and J. J. M. Berdowski (2001), Global emissions sources and sinks, in: Berdowski, J., Guicherit, R., and B.J. Heij (eds.), "The Climate System", pp. 33-78. A.A. Balkema Publishers/Swets & Zeitlinger Publishers, Lisse, The Netherlands. ISBN 90 5809 255 0.

Oshima, N., M. Koike, H. Nakamura, Y. Kondo, N. Takegawa, Y. Miyazaki, D. R. Blake, T. Shirai, K. Kita, S. Kawakami, and T. Ogawa (2004), Asian chemical outflow to the Pacific in late spring observed during the PEACE-B aircraft mission, J. Geophys. Res., 109, D23S05, doi:10.1029/2004JD004976.

Palmer, P. I., D. J. Jacob, D. B. A. Jones, C. L. Heald, R. M. Yantosca, J. A. Logan, G. W. Sachse, and D. G. Streets (2003), Inverting for emissions of carbon monoxide from Asia using aircraft observations over the western Pacific, *J. Geophys. Res.,108(D21)*, 8828, doi:10.1029/2003JD003397.

Piccot, S., J. Watson, and J. Jones (1992), A global inventory of volatile organic compound emissions from anthropogenic sources, *J. Geophys. Res*., *97*, 9897-9912.

Rinsland, C. P., E. Mahieu, R. Zander, P. Demoulin, J. Forrer, and B. Buchmann (2000), Free tropospheric CO, C2H6, and HCN above central Europe: Recent measurements from the Jungfraujoch station including the detection of elevated columns during 1998, *J. Geophys. Res*., *105*, 24,235-24,249.

Rinsland, et al. (2002), Multiyear infrared solar spectroscopic measurements of HCN, CO, C2H6, and C2H2 tropospheric columns above Lauder, New Zealand (45°S latitude), *J. Geophys. Res*., *107*, doi:10.1029/2001JD001150.

Rothman, L. S., et al. (2003), The HITRAN molecular spectroscopic database: Edition of 2000 including updates through 2001, *J. Quant. Spectrosc. Radiat. Transfer*, 82, 5-44.

Singh, H., et al. (2000), Distribution and fate of selected oxygenated organic species in the troposphere and lower stratosphere over the Atlantic, *J. Geophys. Res., 105*, 3795-3805.

Singh, H. B., et al. (2003), In situ measurements of HCN and CH3CN over the Pacific Ocean: Source, sink, and budgets, *108(D20)*, 8795, doi:10.1029/2002JD003006.

Spivakovsky, et al. (2000), Three-dimensional climatological distribution of tropospheric OH: Update and evaluation, *J. Geophys. Res*., 105, 8931-8980.

Streets, D. G., et al. (2003), An inventory of gaseous and primary aerosol emissions in Asia in the year 2000, *J. Geophys. Res*., *108(D21)*, 8809, doi:10.1029/2002JD003093.

Stricker, N. C. M., A. Hahne, D. L. Smith, J. Delderfield, M. B. Oliver, and T. Edwards (1995), ATSR-2, the evolution in its design from ERS-1 to ERS-2, *ESA Bull*., *83*, August 1995.

Tanimoto, H., H. Furutani, S. Kato, J. Matsumoto, Y. Makide, and H. Akimoto (2002a), Seasonal cycles of ozone and oxidized nitrogen species in northeast Asia, 1. Impact of regional climatology and photochemistry observed during RISOTTO 1999-2000, *J. Geophys. Res*., *107(D24)*, 4747, doi:10.1029/2001JD001496.

Tanimoto, H., O. Wild, S. Kato, H. Furutani, Y. Makide, Y. Komazaki, S. Hashimoto, S. Tanaka, and H. Akimoto (2002b), Seasonal cycles of ozone and oxidized nitrogen species in northeast Asia, 2. A model analysis of the roles of chemistry and transport, *J. Geophys. Res*., *107(D23)*, 4706, doi:10.1029/2001JD001497.

Tomikawa, Y., and K. Sato (2005), Design of the NIPR trajectory model, Polar Meteorol. Glaciol., 19, 120-137.

van der Werf, G. R., J. T. Randerson, G. J. Collatz, L. Giglio, P. S. Kashibhatla, A. F. Arellano Jr., S. C. Olsen, and E. S. Kasischke (2004), Continental-scale partitioning of fire emissions during the 1997 to 2001 El Nino/La Nina period, Science, 303, 73-76.

Wang, Y., D. J. Jacob, and J. A. Logan (1998), Global simulation of tropospheric O3-NOx-hydrocarbon chemistry: 1. Model formulation, *J. Geophys. Res*., *103*, 10,713-10,725.

Wang, Y. X., M. B. McElroy, T. Wang, and P. I. Palmer (2004), Asian emissions of CO and NOx: Constraints from aircraft and Chinese station data, *J. Geophys. Res*., *109*, D24304, doi:10.1029/2004JD005250.

Yevich, R., and J. A. Logan (2003), An assessment of biofuel use and burning of agricultural waste in the developing world, *Global Biogeochemical Cycles*, *17*(4), doi:10.1029/2002GB001952.

Yurganov, et al. (2005), Increased Northern Hemispheric carbon monoxide burden in the troposphere in 2002 and 2003 detected from the ground and from space, Atmos. Chem. Phys., 5, 563-573.

Zhao, Y., Y. Kondo, F.J. Murcray, X. Liu, M. Koike, K. Kita, H. Nakajima, I. Murata, and K. Suzuki (1997), Carbon monoxide column abundances and tropospheric concentrations retrieved from high resolution ground-based infrared solar spectra at 43.5 ° N over Japan, *J. Geophys. Res*., 102, 23,403-23,411.

Zhao, Y., Y. Kondo, F.J. Murcray, X. Liu, M. Koike, H. Irie, K. Suzuki, M. Sera, and Y. Ikegami (2000), Seasonal variations of HCN over northern Japan measured by ground-based infrared solar spectroscopy, *Geophys. Res. Lett*., *27*, 2085-2088.

Zhao, Y., K. Strong, Y. Kondo, M. Koike, Y. Matsumi, H. Irie, C. P. Rinsland, N. B. Jones, K. Suzuki, H. Nakajima, H. Nakane, and I. Murata (2002), Spectroscopic measurements of tropospheric CO, C_2H_6, C_2H_2, and HCN, in northern Japan, *J. Geophys. Res*., 107(D18), 4343, doi:10.1029/2001JD000748.

Authors' addresses

N. B. Jones, Department of Chemistry, University of Wollongong, Wollongong, NSW 2522, Australia (njones@uow.edu.au).
M. Koike and H. Matsui, Department of Earth and Planetary Science, Graduate School of Science, The University of Tokyo, Hongo 7-3-1, Bunkyo-ku, Tokyo, 113-0033, Japan (koike@eps.s.u-tokyo.ac.jp, matsui@eps.s.u-tokyo.ac.jp).
Y. Kondo, Research Center for Advanced Science and Technology, University of Tokyo, 4-6-1 Komaba, Meguro, Tokyo 153-8904, Japan (kondo@atmos.rcast.u-tokyo.ac.jp).
Y. Matsumi, Solar-Terrestrial Environment Laboratory, Nagoya University, Toyokawa, Aichi, Japan (matsumi@stelab.nagoya-u.ac.jp).
P. I. Palmer, School of Earth and Environment, University of Leeds, Leeds, LS2 9JT, UK (pip@env.leeds.ac.uk).
H. Tanimoto, National Institute for Environmental Studies, 16-2 Onogawa, Tsukuba, Ibaraki 305-8506, Japan (tanimoto@nies.go.jp).
Y. Zhao, Mechanical and Aeronautical Engineering, University of California, Davis, CA, USA (yjzhao@ucdavis.edu).

Figure Captions

Figure 1. (a) Source regions for "source-labeled" CO tracer simulations. (b) Geographic locations of Moshiri (FTIR), Rikubetsu (FTIR), and Rishiri (in situ) observatories.

Figure 2. Averaging kernels for 0-4- and 0-12-km CO retrievals for solar zenith angles (SZAs) of 30° and 70°. The initial profile for the retrieval analyses is also shown.

Figure 3. (a) Scatter plot of observed daily CO mixing ratio ratios (0-4-km retrievals) between Moshiri and Rikubetsu measurements. A regression line is also shown. (b) Scatter plot of observed daily CO mixing ratios between Moshiri (0-4-km retrievals) and Rishiri (in situ measurements at the surface). A regression line for data with in situ CO concentrations lower than 200 ppbv is also shown.

Figure 4. Daily CO mixing ratios in the year 2001 obtained by FTIR observation (0-4-km retrievals; combined data for Moshiri and Rikubetsu) and corresponding GEOS-CHEM model calculations on days when observed data are available. Model results were vertically smoothed using averaging kernels so that their values can be directly compared.

Figure 5. Monthly averages of CO mixing ratios in the year 2001 obtained by FTIR observation (0-4- and 0-12-km retrievals; combined data for Moshiri and Rikubetsu) and corresponding GEOS-CHEM model calculations. For the model calculations, only the results for days when observed data are available are used after vertical smoothing using averaging kernels.

Figure 6. Ratio of partial column amounts between 0-4- and 0-12-km altitude ranges. For the model calculations, only the results for days when observed data are available are used after the vertical smoothing using averaging kernels.

Figure 7. Scatter plot of daily deviations of CO values from individual monthly averages between observations (0-4-km retrievals) and model calculations (vertical

smoothing). A monthly average is subtracted from individual daily values to eliminate seasonal variations owing to reveal an agreement in day-to-day variations.

Figure 8. Model-calculated daily CO values at a sigma level of 0.902 (about 1 km altitude) at Moshiri-Rikubetsu, in northern Japan. Contributions from various CO sources are also shown. Results for all days in the year 2001 are shown. No smoothing is applied. The notation (source labels) is explained in Table 4.

Figure 9. Model-calculated monthly CO values at a sigma level of 0.902 (about 1 km altitude) at Moshiri-Rikubetsu, in northern Japan. Contributions from various CO sources are also shown. The notation (source label) is explained in Table 4. Results for all days in the year 2001 are used.

Figure 10. Vertical profile of model-calculated monthly averaged CO values at Moshiri-Rikubetsu, in northern Japan in January and July. Contributions from various CO sources are also shown. The notation (source label) is explained in Table 4. Results for all days in the year 2001 are used.

Figure 11. Monthly mean horizontal wind field at 925 hPa (≈1 km) in January and July (ECMWF 2.5° × 2.5° grid data). The geographic location of Moshiri observatory is also shown (closed circle).

Figure 12. Back trajectories of air parcels arriving at Moshiri at 1 km altitude in January and July. Trajectories for individual days are shown. Color coding shows the atmospheric pressure of air parcels along the trajectories.

Figure 13. Map showing integrated CO emissions that individual air parcel received within individual grid boxes along trajectories in January and July. The total time duration in which individual air parcels existed in each grid box at altitudes below the 800-hPa level was calculated and it was multiplied by the CO emissions for this particular grid box.

Figure 14. Hot spots detected by ATSR satellite measurement in April 2001 and back trajectories of air parcels arriving at Moshiri at 1 km altitude. Trajectories are shown for only one for every three days.

Figure 15. Scatter plot between observed daily CO mixing ratios (0-12-km retrievals) and daily HCN mixing ratios (0-12-km retrievals) at Moshiri for selected months. Different symbols are used for individual months so that changes due to seasonal variations of CO and HCN are minimized. A slope of enhancements (anomalies from the normal seasonal variation) between HCN and CO (ΔHCN/ΔCO) calculated for data obtained in the years 1998 and 2002 using the method described by *Zhao et al*. [2002] is also shown (heavy solid line).

Table 1. Microwindows used for CO and HCN retrievals

Line identification	Line Center (cm^{-1})	Spectral Region (cm^{-1})	Interfering Absorption
†CO(1-0) P(10)	2057.8575	2057.684-2058.0	O_3, CO_2, OCS
†CO(1-0) P(7)	2069.6559	2069.56-2069.76	O_3, CO_2, OCS
*CO(6-5) R(32)	2112.1452	2112.08-2112.18	O_3
HCN (3-0) P(14)	3268.2229	3268.18-3268.27	$H_2{}^{17}O$, $H_2{}^{18}O$
HCN (3-0) P(8)	3287.2483	3268.18-3268.27	
HCN (3-0) P(4)	3299.5273	3299.46-3299.58	H_2O, O_3

† The absorption is due to the isotope $^{13}C^{16}O$.

* The absorption is due to solar CO.

Table 2. Error budget for CO and HCN retrievals (%)

	CO		HCN
	0-4 km	0-12 km	0-12 km
Systematic Error			
Forward model approximation	4	4	2
Spectroscopic parameters	2	2	5
Instrumental line shape	1.2	1.2	1
A priori profile	20	6	15
Total (RSS)	21	7.6	16
Random Error			
Spectral noise	4	2	6
SZA	<1	<1	<1
Temperature	4.2	4.2	3.2
Interference	<1	<1	<1
Total (RSS)	6.0	4.9	6.9

Table 3. Monthly average CO mixing ratios in the year 2001 obtained by FTIR observations (combined data for Moshiri and Rikubetsu)

		CO 0~4 km (ppbv)		CO 0~12 km (ppbv)	
Month	N	Average	σ	Average	σ
1	7	165	8	131	7
2	9	175	9	137	6
3	8	189	12	149	11
4	8	192	12	152	9
5	16	189	18	152	15
6	9	173	18	141	15
7	8	145	10	120	7
8	12	155	15	128	12
9	13	136	16	111	12
10	14	150	21	118	14
11	10	141	8	112	6
12	0	------	------	-------	------

Table 4. Results from source-labeled model calculation of CO at sigma levels of 0.902 and 0.464 (about 1 and 6 km altitude) at Moshiri-Rikubetsu.

Source	Contribution (%)					
	σ =0.902			σ =0.464		
	Yearly Average	January	July	Yearly Average	January	July
Fossil Fuel						
Asia (AS_FF)	30.9	22.8	44.9	19.3	22.1	19.8
Europe (EU_FF)	17.7	27.5	3.9	13.1	15.6	9.8
North America (NA_FF)	8.8	13.0	2.5	11.6	14.4	6.6
Other (Other_FF)	1.7	3.1	0.6	2.7	3.8	1.3
Biomass Burning						
Asia (AS_BB)	5.8	2.0	5.9	5.7	2.4	8.5
Africa (AF_BB)	1.4	1.7	0.7	3.0	3.2	1.5
South America (SA_BB)	0.6	0.7	0.4	1.3	1.1	0.9
Other (Other_BB)	2.5	1.6	1.7	2.4	1.6	3.6
Chemical Production	30.6	27.6	39.4	41.0	35.8	48.0

Figure1

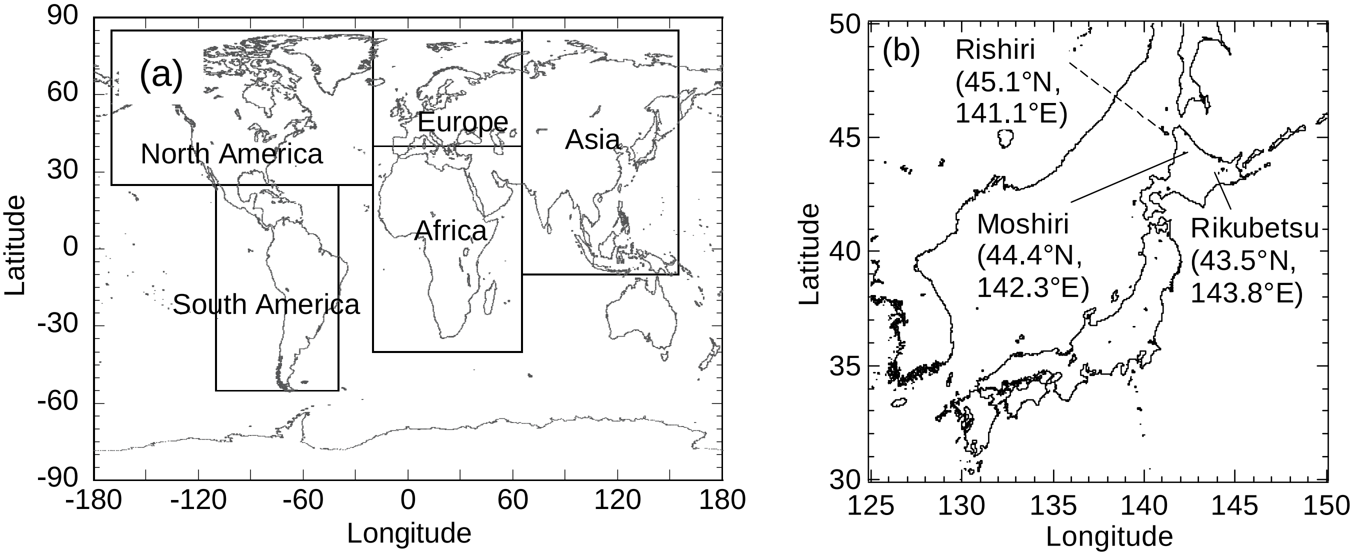

Figure2

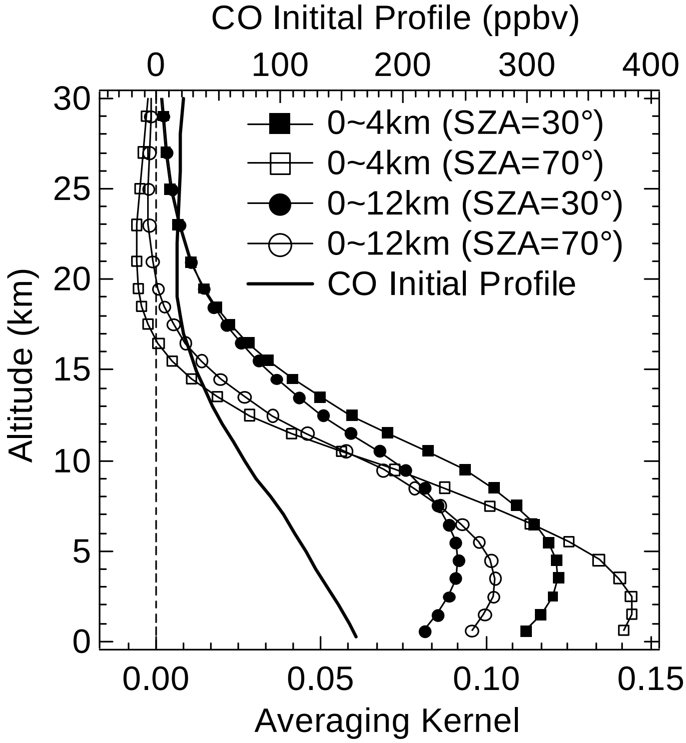

Figure3

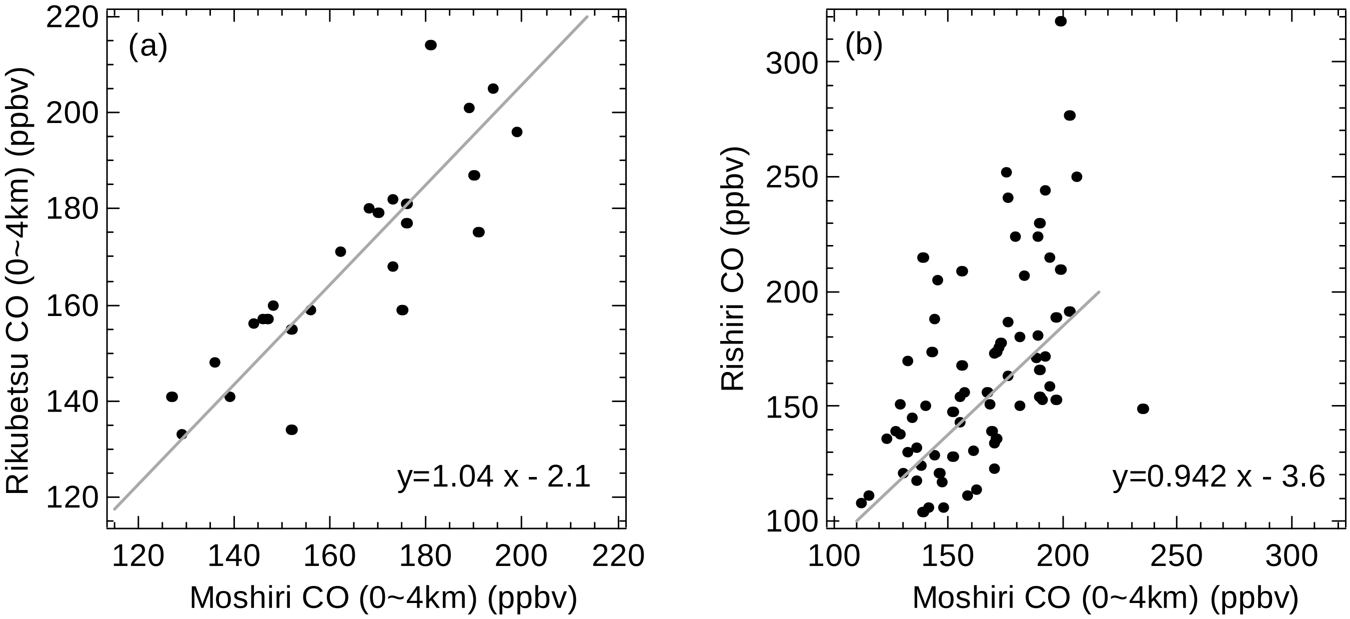

Figure4

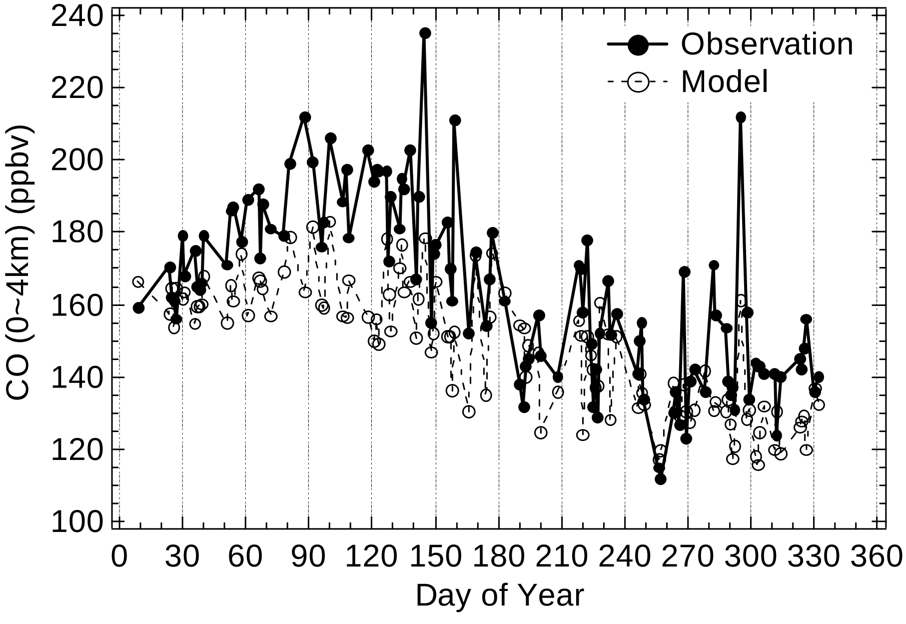

Figure5

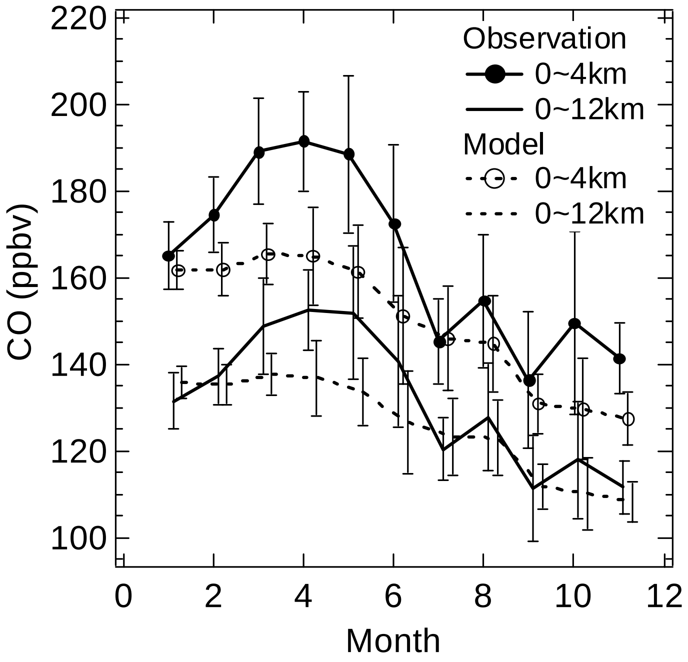

Figure6

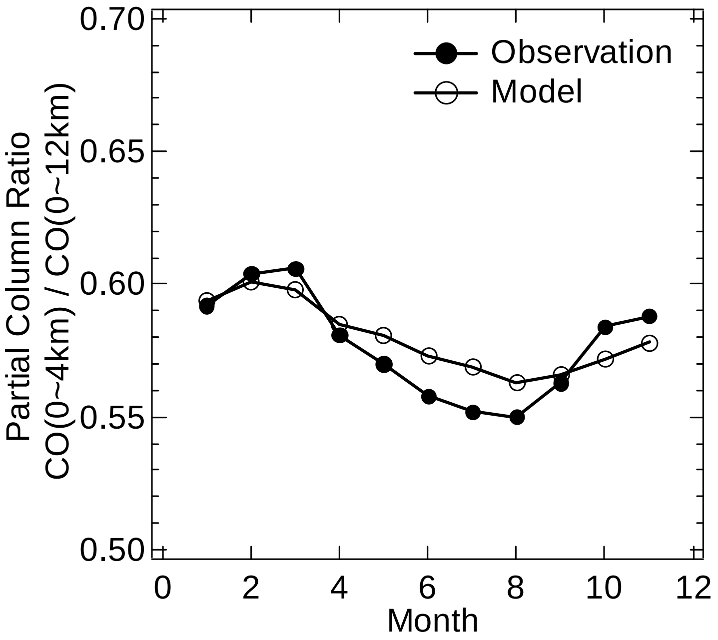

Figure7

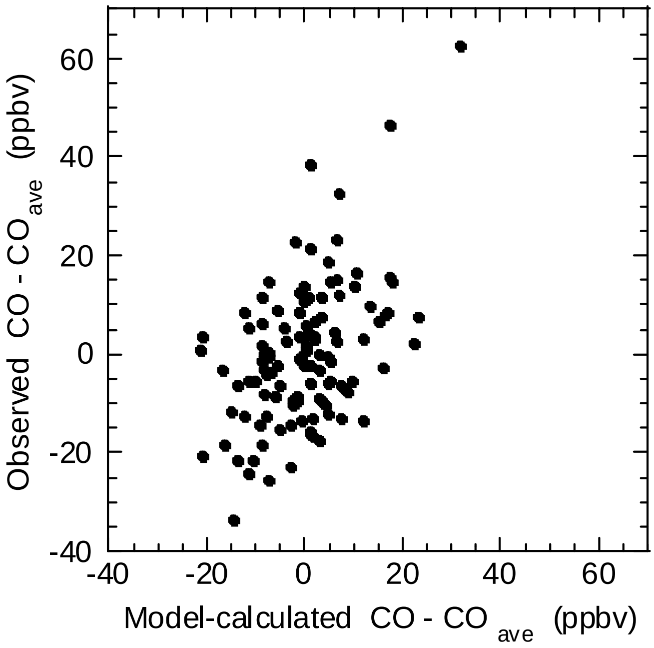

Figure8

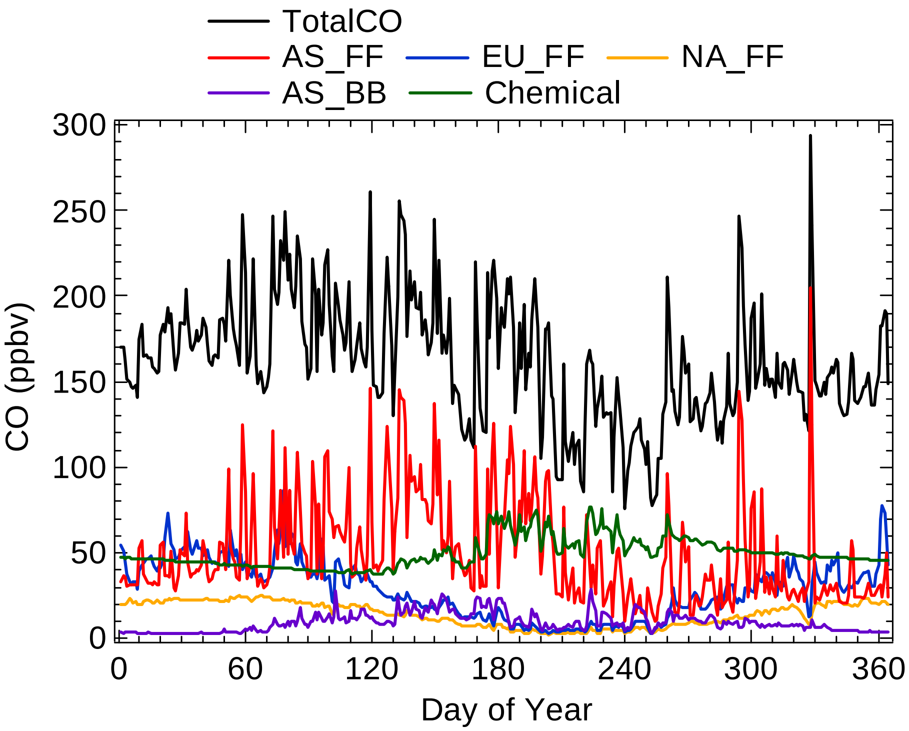

Figure9

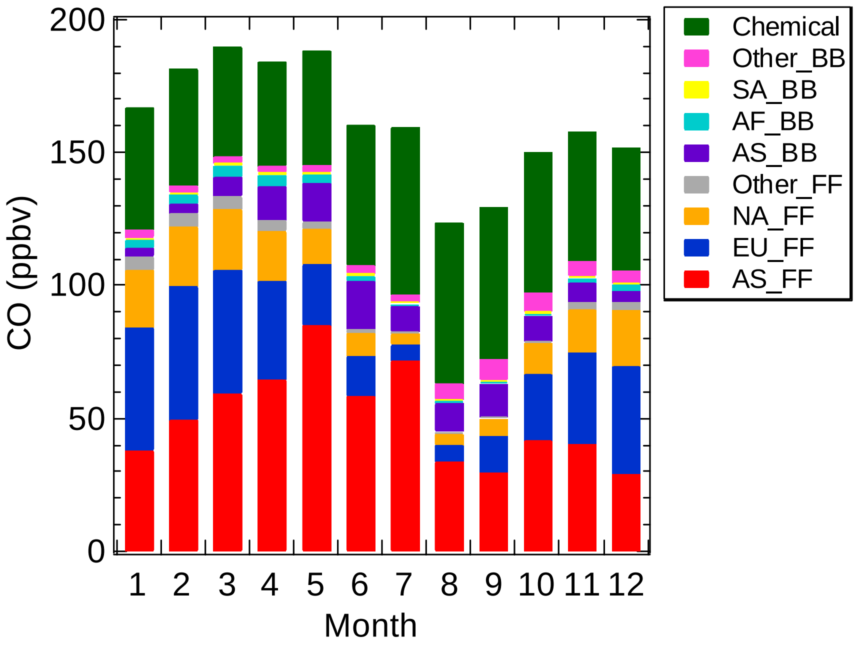

Figure10

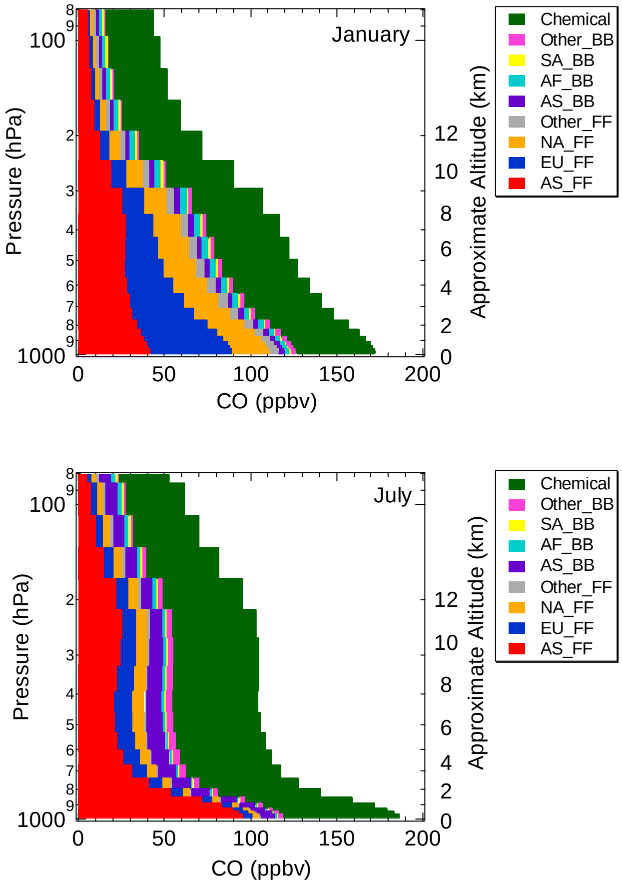

Figure11

(a) JAN 2001 Mean Wind at 925 hPa

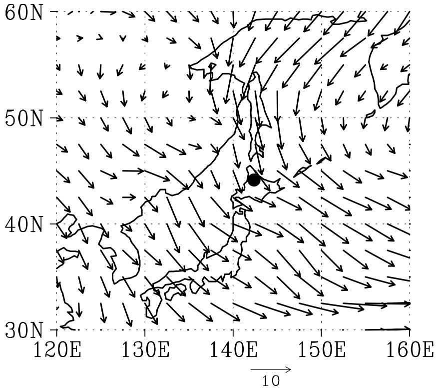

(b) JUL 2001 Mean Wind at 925 hPa

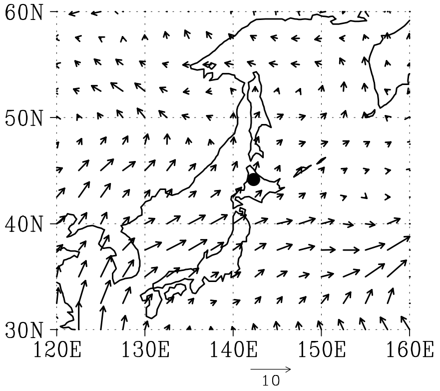

Figure12

January 2001 1km

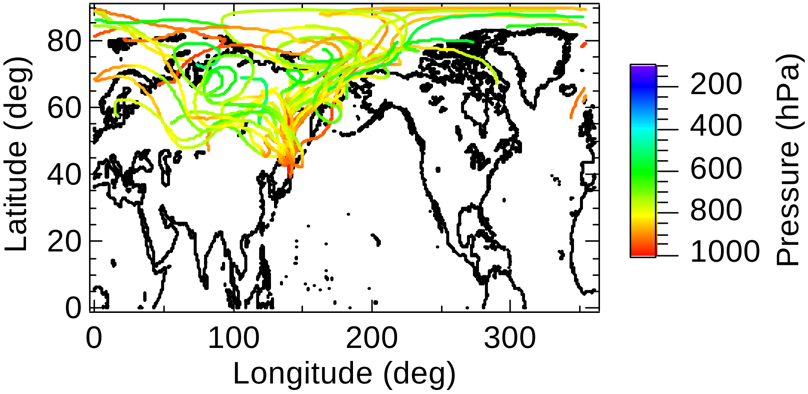

July 2001 1km

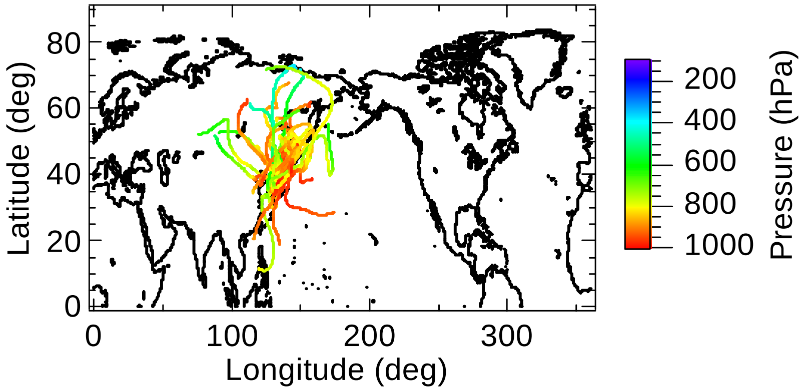

Figure13

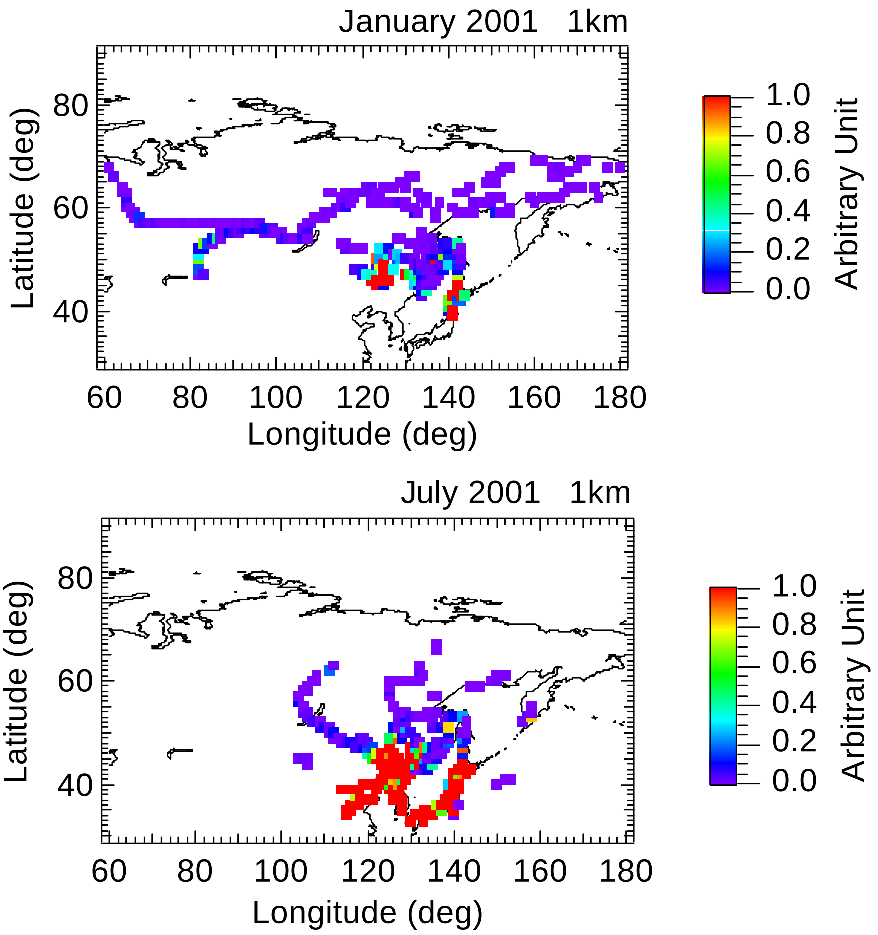

Figure14

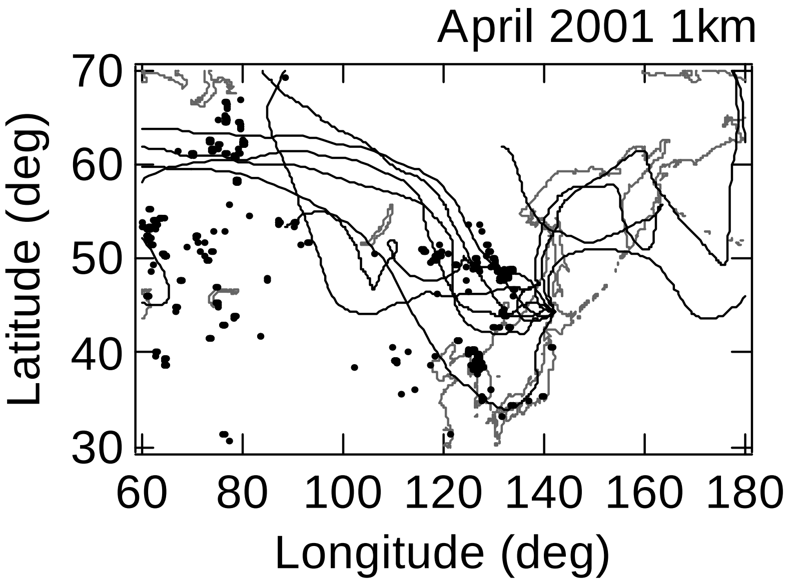

Figure15

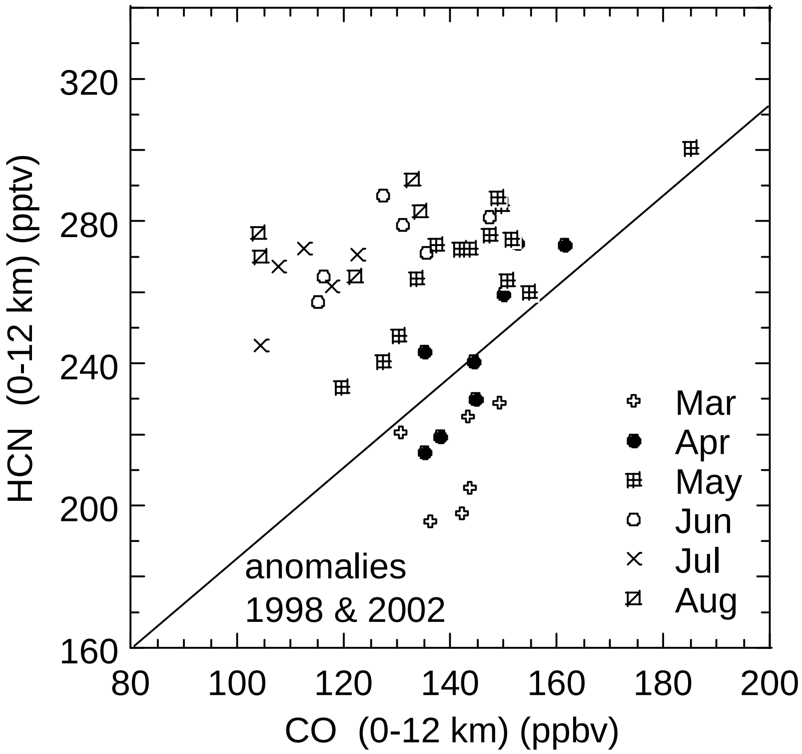
320
280
240
200
160
80
100
120
140
160
180
200
HCN (0-12 km) (pptv)
CO (0-12 km) (ppbv)
anomalies
1998 & 2002
Mar
Apr
May
Jun
Jul
Aug